Check for updates



www.chemsuschem.org

Sustainable Gas Storage: CO₂ Activation of Edge-Functionalized Graphitic Nanoplatelets

Seok-Jin Kim,^[a, b] Min Hui Kim,^[c] Se Jung Lee,^[c] Cafer T. Yavuz,*^[a, b] and In-Yup Jeon*^[c]

Graphitic nanoplatelets (GnPs), edge-selectively carboxylated graphitic nanoplatelets (ECGnPs), are functionalized with a carboxylic acid at the edge increasing their surface area, and are highly dispersible in various solvents. However, there is a limit in that the basal plane remains intact because it is functionalized only in the part where the radical is generated at the edge. Here, we activate ECGnPs to have porous structures by flowing CO_2 at $900\,^{\circ}\mathrm{C}$. Etching of the ECGnPs structure was

performed through the Boudouard reaction, and the surface area increased from $579 \, \text{m}^2 \, \text{g}^{-1}$ to a maximum of $2462 \, \text{m}^2 \, \text{g}^{-1}$. In addition, the pore structure was investigated with various adsorption gases (CH₄, Ar, CO₂, H₂, and N₂) according to the reaction time. This study provides the overall green chemistry in that it utilizes CO₂ from manufacturing to activation compared to the process of activating with conventional chemical treatment.

1. Introduction

The functionalization of carbon materials through ball milling has gained significant attention since 2012 for diverse energyrelated applications, encompassing thermochemical catalysts, electronic devices, supercapacitors, electrodes, flame retardants, and electrocatalysts.[1-8] In ball milling, the mechanical energy generated by steel balls disrupts carbon bonds, forming functionalized radicals that readily bind with adjacent reactants.[1-2] This method offers the advantage of transforming low-cost graphite into high-quality material through a straightforward manufacturing process, making it an attractive candidate for mass production and industrial applications. However, the limitations of ball milling lie in its selective functionalization at radical sites, leaving the basal plane relatively untouched, thereby restricting its versatility.^[4] As a result, most ball-milled carbon (BMC) materials have mainly found use as electrochemical catalysts by forming metal complexes. [9]

To broaden the utilization of BMC material, novel approaches are necessary to modify and enhance their properties. Traditional carbon activation methods involve chemical treatments such as wet oxidation, utilizing agents like phosphoric acid (H_3PO_4), zinc chloride ($ZnCl_2$), sodium hydroxide (NaOH), potassium carbonate (K_2CO_3), potassium hydroxide (COH_3), phytic acid ($C_6H_{18}O_{24}P_6$), etc. COH_3 0 Among them, KOH is the most effective chemical treatment method.

KOH is known to be highly corrosive, hazardous to human health, and can cause damage to reactors at high temperatures. [17–18] Moreover, generating carbon dioxide (CO₂) during the activation process raises environmental concerns, making it far from an environmentally friendly manufacturing approach. [10]

In light of these challenges, this study proposes an environmentally friendly carbon activation technique that intertwines carbon usage with climate change mitigation technology. We prepared edge-selectively carboxylated graphitic nanoplatelets (ECGnPs) by ball-milling graphite with CO₂. Subsequently, the ECGnPs underwent heat treatment in a CO₂ atmosphere to produce activated ECGnPs (Act-GnPs) with an impressive surface area of up to 2418 m² g $^{-1}$. Gas adsorption experiments demonstrated the variable pore widths of Act-GnPs, reflecting their response to the treatment time. This study showcases the efficiency of CO₂ activation as an alternative to conventional chemical treatments and expands the potential applications of BMC materials in gas storage.

The significance of this research lies in its contribution to developing a sustainable and efficient method for activating carbon materials. The $\rm CO_2$ activation process increases the surface area of graphitic nanoplatelets (GnPs) and offers a greener alternative to chemical activation methods that rely on harsh chemicals. Furthermore, the increased surface area and tunable pore structure of Act-GnPs open new possibilities for gas storage and separation applications. By understanding the $\rm CO_2$ activation mechanism and its effect on the properties of GnPs, this study paves the way for the utilization of Act-GnPs in various energy-related applications.

Overall, this research presents a novel approach to activating GnPs using CO_2 , offering significant advantages over conventional methods and promising potential for industrial-scale production and widespread applications in gas storage and separation technologies.

[[]a] S.-J. Kim, C. T. Yavuz Advanced Membranes & Porous Materials Center (AMPMC), King Abdullah University of Science and Technology (KAUST), Thuwal 23955, Saudi Arabia E-mail: cafer.yavuz@kaust.edu.sa

[[]b] S.-J. Kim, C. T. Yavuz KAUST Catalysis Center (KCC), King Abdullah University of Science and Technology (KAUST), Thuwal 23955, Saudi Arabia

[[]c] M. Hui Kim, S. Jung Lee, I.-Y. Jeon Department of Chemical Engineering/Nanoscale Environmental Sciences and Technology Institute, Wonkwang University, 460 Iksandae-ro, Iksan, Jeonbuk 54538, Republic of Korea E-mail: iyjeon79@wku.ac.kr

2. Materials and Methods

2.1. Synthesis of Edge-Selectively Carboxylated Graphitic Nanoplatelets (ECGnPs)

The pristine graphite (80 g×4, 32 mesh, Sobaek industry, Inc.) and 5 mm diameter stainless steel balls (1.0 kg) were put into a container. After removing the air completely, the container was charged with CO_2 (4 MPa). Then, the container was fastened to a planetary ball mill (Pulverisette 5, Fritsch) and operated at 350 rpm for 48 h. The resulting material was collected and treated with a 1.0 M aq. HCl solution to completely remove the unbound metallic residue. The purified products were freezedried at $-120\,^{\circ}$ C under reduced pressure (0.05 mmHg) for 48 h to obtain 365.6 g of a dark black powder (ECGnPs).

2.2. Activation of the ECGnPs

The pristine ECGnPs (10.0 g) were loaded into a horizontal quartz tube furnace, and a high-purity (99.995%) CO₂ feed gas was controlled by a calibrated mass controller (MKP, South Korea). The heat treatment was conducted at a ramping rate of 10 °C min⁻¹ to 900 °C under a continuous CO₂ flow. The activation time was screened at 2-hour intervals from 2 to 8 h, and comparative experiments were performed by changing the feed gases (N₂, H₂O), flow rate (100–500 mLmin⁻¹), and temperatures (700–900 °C). At a flow rate of 300 mLmin⁻¹ and a temperature of 900 °C, the yields of activated GnPs were collected as 7.17 g, 6.62 g, 4.49 g, and 3.15 g for activation times of 2, 4, 6, and 8 hours, respectively.

2.3. General Characterization

Powder X-ray diffraction (PXRD) studies were conducted with a High-Power X-Ray Diffractometer D/MAX2500 V/PC (Cu–K α radiation, 40 kV, 200 mA, λ =1.54056 Å) (Rigaku Inc., Japan). Elemental analysis was conducted with a Flash 2000 Analyzer (Thermo Scientific Inc., USA). N_2 adsorption isotherms at 77 K were measured with a Micromeritics 3Flex surface characterization analyzer (Micromeritics Instruments, Norcross, GA, USA), and the surface areas of each sample were calculated using the Brunauer-Emmett-Teller (BET) method within the consistency criteria. The Raman spectra were collected from a LabRAM HR

Evolution spectrometer (Horiba Inc., Japan). Fourier transform infrared (FT-IR) analysis used Spectrum 100 (PerkinElmer Inc., USA). The methane, carbon dioxide, argon, and hydrogen adsorption isotherms were also measured with the 3Flex analyzer. Thermogravimetric analysis (TGA) was conducted in an air atmosphere at a ramping rate of 10°Cmin⁻¹ with a STA 8000 (PerkinElmer Inc., USA). Scanning electron microscope (SEM) images were taken with a Field Emission Scanning Electron Microscope Nanonova 230 (FEI Inc., USA) at 10 kV and 0.16 nA. High-resolution transmission electron microscopy (HR-TEM) was done with a JEM-2100F microscope (JEOL Inc., Japan) under an operating voltage of 200 keV.

3. Results and Discussion

The pristine ECGnPs were manufactured by ball-milling with graphite and CO₂ (see Materials and Methods). To activate the ECGnPs with CO₂, they were placed in a quartz tube, and the temperature was raised slowly ($10\,^{\circ}\text{Cmin}^{-1}$) under a CO₂ flow (Figure 1). The optimization of the CO₂ activation process was investigated by gradually increasing the temperature from 700 to 900 °C, and it was found that the highest specific surface area (SSA) of 950 m²g⁻¹ was achieved at 900 °C with a CO₂ flow rate of 100 mL min⁻¹ (Table 1). The increase in surface area was attributed to the Boudouard reaction (C+CO₂→2CO), which develops the pore structure at temperatures above 800 °C. ^[19]

To further examine the effect of the flow rate, we varied the CO_2 flow rate from 300 to 500 mL min $^{-1}$ with a gas hourly space velocity (GHSV) of 9,000 and 15,000 mL g^{-1} h $^{-1}$, respectively. However, the change in surface area within this range was not remarkable (Table 1), so the optimum treatment time was determined based on a flow rate of 300 mL min $^{-1}$. The CO_2 activation was performed at 900 °C, and the SSA of the ActGnPs gradually increased until 6 hours of CO_2 treatment (2462 m 2 g $^{-1}$) and then decreased (Figure 2). This indicated that the pore structure developed as the carbon structure was etched by CO_2 . However, prolonged treatment time led to a collapse of the pore structure due to excessive Boudouard reaction. Thus, selecting an appropriate treatment time is crucial for efficient carbon activation.

Structural analysis was performed to understand the CO_2 activation mechanism for ECGnP (Figure 3a). The ECGnPs prepared under a CO_2 atmosphere have hydrophilic functional groups (-OH, -CHO, -COOH, -C-O-C-, -C=O, etc.) at the edge,

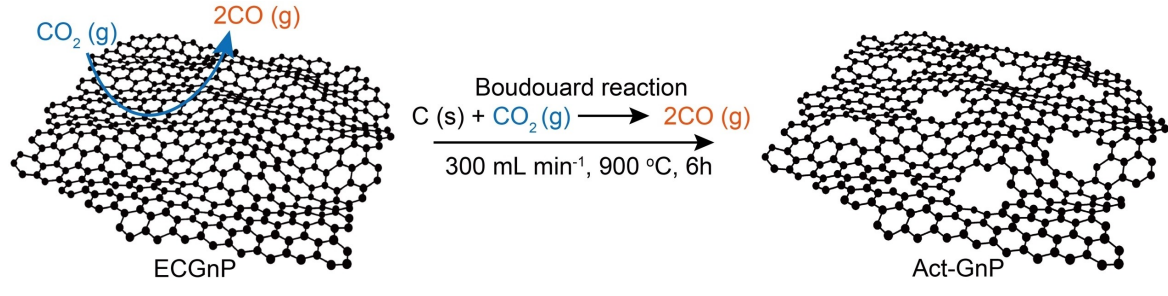


Figure 1. Schematic showing the procedure for the CO₂-activated graphitic nanoplatelets (Act-GnPs).



Table 1. The specific surface area (SSA) changes of the pristine graphite (without ball milling) and EXGnPs (X=C, N, and P) according to the activation conditions.							
Sample	Gas	Gas Flow (mL/min)	Temperature (°C)	Time (h)	BET surface area (m²/g)		
Graphite	-	-	-	-	5.5		
ECGnP	-	-	-	-	579		
	N_2	100	900	2	662		
	H ₂ O	100	900	2	912		
	CO ₂	100	900	2	950		
			800	2	772		
			700	2	730		
		300	900	2	1184		
				4	1397		
				6	2462		
				8	1654		
		500	900	2	1210		
ENGnP	-	-	-	-	256		
	CO_2	100	700	2	340		
		100	800		577		
		100	900		1026		
EPGnP	-	-	-	-	469		
	CO ₂	100	900	2	1000		
		300	900	1	926		

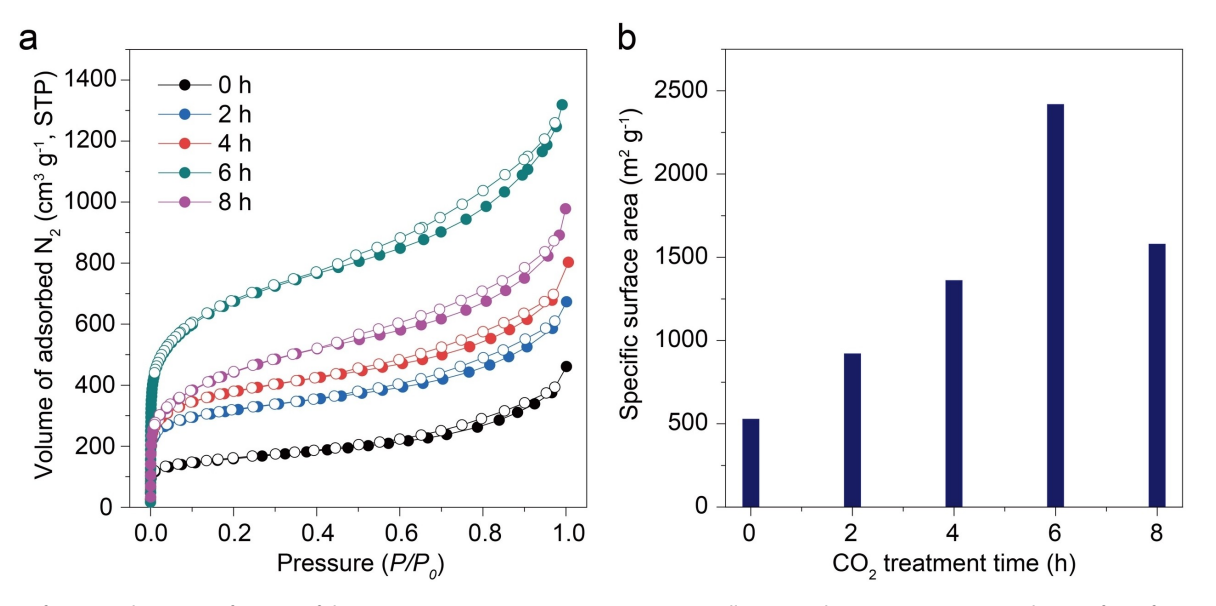


Figure 2. Surface area change as a function of the CO_2 treatment time: a) Brunauer-Emmett-Teller (BET) adsorption curves at 77 K; b) Specific surface area (SSA, m^2g^{-1}) from N_2 adsorption.

which were removed during the heat treatment, resulting in a decrease in oxygen content. Elemental analysis (EA) confirms that the oxygen ratio drops rapidly after the heat treatment (Figure 3b inset) due to the removal of functional groups and dangling bonds. The thermal stability of Act-GnPs was stable up to 500°C under an air atmosphere, and this stability was significantly influenced by the presence or absence of oxygen-

containing functional groups (Figure 3b). To elucidate the changes in carbon structures over time due to CO_2 activation, Raman spectroscopy analysis was also performed (Figure 3c). Before the CO_2 treatment, the I_D/I_G ratio was at its lowest, but as the CO_2 treatment proceeded, the D band area increased, showing the highest I_D/I_G ratio at 6 hours before decreasing again from 8 hours onwards. This suggests that initial CO_2

15, Downloaded from https://themistry-europe.onlinelibrary.wiley.com/doi/10.1002/cssc.202301145 by King Abdullah Univ. Of Science & Tech Kaust, Wiley Online Library on [03/11/2025]. See the Terms and Conditions (https://onlinelibrary.wiley.com/terms-and-conditions) on Wiley Online Library for rules of use; OA articles are governed by the applicable Creative Common of the Common

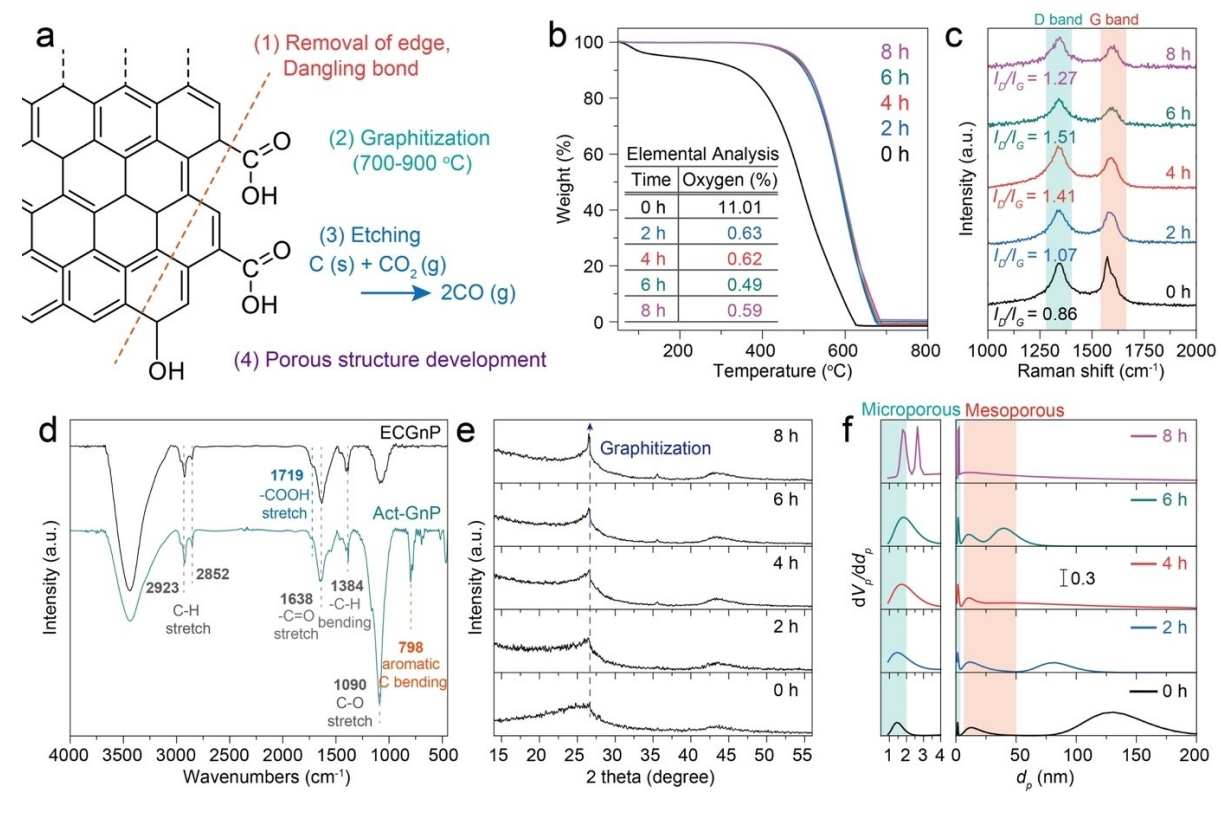


Figure 3. Characterization of the Act-GnPs according to the CO₂ treatment times: a) Schematic representation of the CO₂ activation mechanism for the ECGnPs; b) Thermogravimetric analysis (TGA) of the Act-GnPs in the air (inset: elemental analysis (EA) of oxygen contents in the Act-GnPts); c) Raman spectra and their D (cyan), G (orange) bands of Act-GnPs with I_D/I_G ratio. d) Fourier-transform infrared (FT-IR) spectra of the ECGnPs (0 h) and Act-GnPs (6 h); e) XRD patterns of the Act-GnPs; f) Pore size distribution of the Act-GnPs derived by non-local density functional theory (NLDFT) from Ar adsorption at 87 K.

treatment introduces defects into the basal plane structure of GnPs, forming a porous structure, and over time, this process extends to further degrade the structure. This observation is highly consistent with the trends found in the BET results of Figure 2. Additionally, the significant decomposition of carbon structure is indicated by a subtle increase in the O/C ratio in the EA result at 8 hours (Figure 3b inset). Fourier-transform infrared (FT-IR) spectra confirmed the reduction of the carboxyl acid group (-COOH, 1719 cm⁻¹) of ECGnPs and the increase in the aromatic C- bending peak after heat treatment (Figure 3d).

At 900 °C, graphitization occurred, leading to the development of the graphitic layer. X-ray diffraction (XRD) patterns showed that the graphitic layer continued to grow with increased processing time (Figure 3e). This graphitization is not very advantageous from a surface area point of view. While graphitization improved the electrical conductivity and structural stability, it also reduced the surface area due to the development of a narrow graphitic layer. The comparison with $\mbox{N}_2\mbox{-treated}$ ECGnPs confirmed that \mbox{CO}_2 activation exhibited higher surface area improvement (950 m² g⁻¹) compared to N₂ (inert) treatment (662 m² g⁻¹) (Table 1). This suggested that CO₂ activation effectively developed the pore structure while simultaneously etching the carbon structure during the graphitization process.

In the case of pristine graphite without ball milling, the CO₂ treatment did not significantly increase surface area (5.5 m² g⁻¹, Table 1). This can be attributed to the fact that the ball milling process functionalizes the carbon edge, widening the interlayer distance and creating opportunities for gases to permeate and etch the carbon structure. As a result, ball milling plays a crucial role in enhancing the CO₂ activation process, enabling the development of a high surface area for the Act-GnPs. The ball milling process creates defects and functional groups at the edges of the graphite nanoplatelets, making them more susceptible to CO₂ activation. These functional groups, such as -OH, -CHO, -COOH, -C-O-C-, -C=O, among others, act as active sites for CO2 adsorption and etching, leading to the expansion of the interlayer distance and the development of the pore structure. On the other hand, pristine graphite lacks these functional groups, resulting in limited interaction with CO₂ and limited etching capability, thus failing to achieve a significant increase in surface area through CO₂ treatment alone.

Therefore, the combination of ball milling and CO₂ activation is crucial for obtaining high-performance Act-GnPs with a large surface area, making them suitable for various gas storage and separation applications. The functionalization of graphite through ball milling provides a promising approach to creating tailored carbon materials with enhanced properties for diverse energy-related applications.

To examine the differences according to the functionalization of the graphite with a ball mill, we prepared ENGnPs (edge-nitrogen graphitic nanoplatelets) and EPGnPs (edgephosphorus graphitic nanoplatelets) by ball milling with N₂ and P₂O₅, respectively.^[1,20-21] Subsequently, CO₂ activation was performed under the same condition. After the activation, the specific surface areas (SSAs) of the pristine ENGnPs (256 m² g⁻¹) and EPGnPs (469 m²g⁻¹) were substantially increased up to 1026 m²g⁻¹ and 926 m²g⁻¹, respectively (Table 1). For reference, the ENGnPs, when ball-milled, tend to incorporate a considerable amount of iron, [2] which leads to a significant decrease in carbon yield at high CO₂ flow rates; consequently, screening was conducted only at a flow rate of 100 mL min⁻¹. On the other hand, EPGnPs were processed for merely one hour at a flow rate of 300 mLmin⁻¹. This demonstrated that the ball milling and CO₂ activation allowed for preparing graphitic nanoplatelets with high surface area and incorporating heteroatoms, enabling fine-tuning their properties.

In the case of the N_2 adsorption-desorption isotherm, the quadrupole moment leads to specific interactions with functional groups. These interactions between the N_2 molecule and the surface functionality of the material can shift the pore-filling pressure, leading to inaccuracies in the pore size calculation. To overcome this limitation, the pore structure analysis used

monoatomic argon (Ar) adsorption at 87 K, which lacks dipole or quadrupole interactions. The non-linear density functional theory (NLDFT) approach revealed that the mesopore area decreased micropore area increased as the activation time increased (Figure 3f). The Act-GnPs treated for 6 hours, exhibiting the highest surface area, demonstrated uniformly grown micro- and mesopores. However, after 8 hours, the mesopore region becomes mostly etched leaving only the micropore region. This observation indicated that graphitization and carbon etching occurred concurrently during the $\rm CO_2$ -activation process, allowing for fine-tuning pore size and surface area by selecting an appropriate treatment time.

The morphological changes of the Act-GnPs with heat treatment were visualized using SEM (Figure 4a). The microstructure developed as the activation time increased, enhancing electrical conductivity and structural stability. Looking at the ECGnPs in the TEM image (Figure 4b) shows that most of the deformation occurred around the edge, one of the ball milling characteristics.

After the CO₂ treatment, the partially graphitized region was distributed on the basal plane, indicating a mixture of amorphous and graphitic layers (Figure 4c). This high porosity

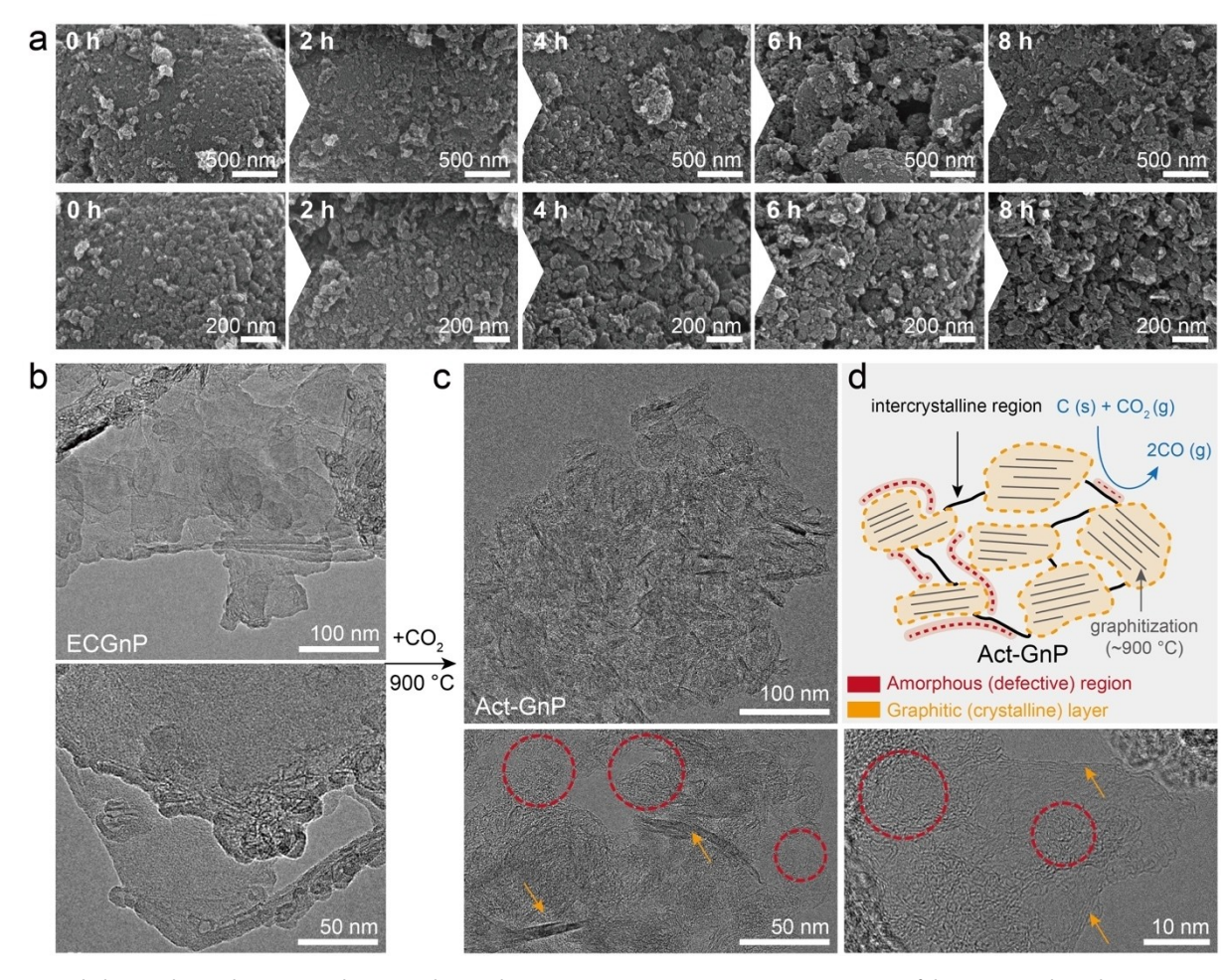


Figure 4. Morphology and gas adsorption analysis according to the CO_2 treatment time at 900 °C. a) SEM images of the ECGnPs (0 h) and Act-GnPs (2, 4, 6, and 8 h). High-resolution TEM images: b) ECGnPs and c) Act-GnPs (6 h). d) Structural changes in Act-GnP during CO_2 activation. The amorphous region is marked in dark red, and the graphical layer is marked in yellow.

after CO_2 activation could be attributed to the even mixing of rigid graphitic layers (size of 10–50 nm) with amorphous carbon structures, preserving nanopores. Figure 4d briefly shows graphitization and the Boudouard reaction occurring simultaneously.

Gas adsorption analysis demonstrated that the adsorption amounts of H_2 , CH_4 , and CO_2 on Act-GnPs increased with increasing activation time for all gases tested (Figure 5a). Interestingly, the optimal activation time differed for each gas, implying that the activation time selectively influenced the surface chemistry and pore structure of Act-GnPs. The highest gas adsorption was observed for CO_2 on the Act-GnPs treated for 2 h, and CH_4 showed the highest adsorption on the Act-GnPs treated for 4 h, while N_2 (representing the highest SSA) and H_2 showed the highest adsorption on the Act-GnPs treated for 6 and 8 h, respectively.

Additionally, the heat of adsorption varied with each treatment time (Table 2), suggesting the potential for selective use in gas separation processes such as pressure swing adsorption (PSA). The pore width increased from 0.6 nm to 1.0 nm as the CO_2 treatment time increased, which is interpreted as the CO_2 molecule having sufficient kinetic energy and reaching a microstructure between the graphitic layers for etching (Figure 5b). Figure 5 presents the gas type and

corresponding pore width (nm) that yielded the highest adsorption amount as a function of the heat treatment time. Notably, this trend is interpreted as independent of the pore size and the kinetic diameter of the gas molecules (CH₄: 380 pm; N₂: 364 pm; CO₂: 330 pm; H₂: 289 pm). However, the non-uniformity in grain size and pore size due to CO₂ activation's random defect formation and the Boudouard reaction's inherent nature limited a comprehensive exploration of the relationship between kinetic diameter and pore size of Act-GnPs.

Despite these challenges, CO₂-activated GnPs (Act-GnPs) demonstrated high gas adsorption capacity, making them promising materials for gas storage and separation applications. Furthermore, the environmentally friendly nature of CO₂ activation, avoiding harsh chemicals and energy-intensive processes, adds to the appeal of this method. Additionally, using waste CO₂ in the activation process contributes to reducing carbon emissions and mitigating climate change. As a result, CO₂-activated BMCs offer exceptional gas adsorption performance and hold great potential for contributing to a more sustainable future (Figure 6).

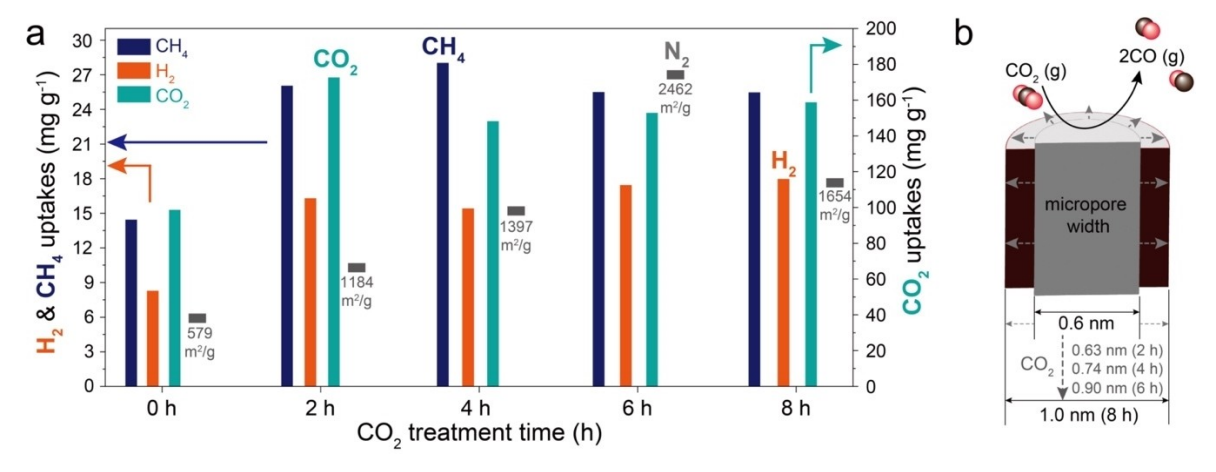


Figure 5. A graph of the change in pore width and the recommended maximum adsorption amount for each treatment time at 900 °C. a) A bar graph comparing the adsorption amount of H_2 at 77 K, CH_4 at 273 K, and CO_2 at 273 K. The surface area (m^{2g-1}) obtained by N_2 adsorption is marked with a gray bar. b) Schematic diagram of pore width changes according to CO_2 treatment time.

Table 2. The adsorption amount (mg g^{-1}) and heat of adsorption (Q_{st}) of CH₄ (273 K), CO₂ (273 K), and H₂ (77 K) of the Act-GnPs according to the CO₂ treatment time (h).

Time (h)	Gas adsorption amount (mg/g)			Heat of adsorption energy (Q_{st}) (kJ/mol)		
	CH ₄	CO ₂	H_2	CH ₄	CO ₂	H ₂
0	14.45	98.70	8.28	23.43	27.81	6.58
2	26.06	172.63	16.32	22.35	27.29	7.12
4	28.03	148.23	15.43	19.72	25.87	5.59
6	25.50	152.89	17.46	19.63	23.28	6.32
8	25.47	158.79	18.00	20.15	24.33	6.98

 \times The heat of adsorption (Q_{st}) was calculated with the adsorption amounts at 298 K (CH₄, CO₂) and 87 K (H₂), respectively.

//chemistry-europe.onlinelibrary.wiley.com/doi/10.1002/cssc.202301145 by King Abdullah Univ. Of Science & Tech Kaust, Wiley Online Library on [03/11/2025]. See the Terms and Conditions (https://onlinelibrary.

ditions) on Wiley Online Library for rules of use; OA articles are governed by the applicable Creative Comm

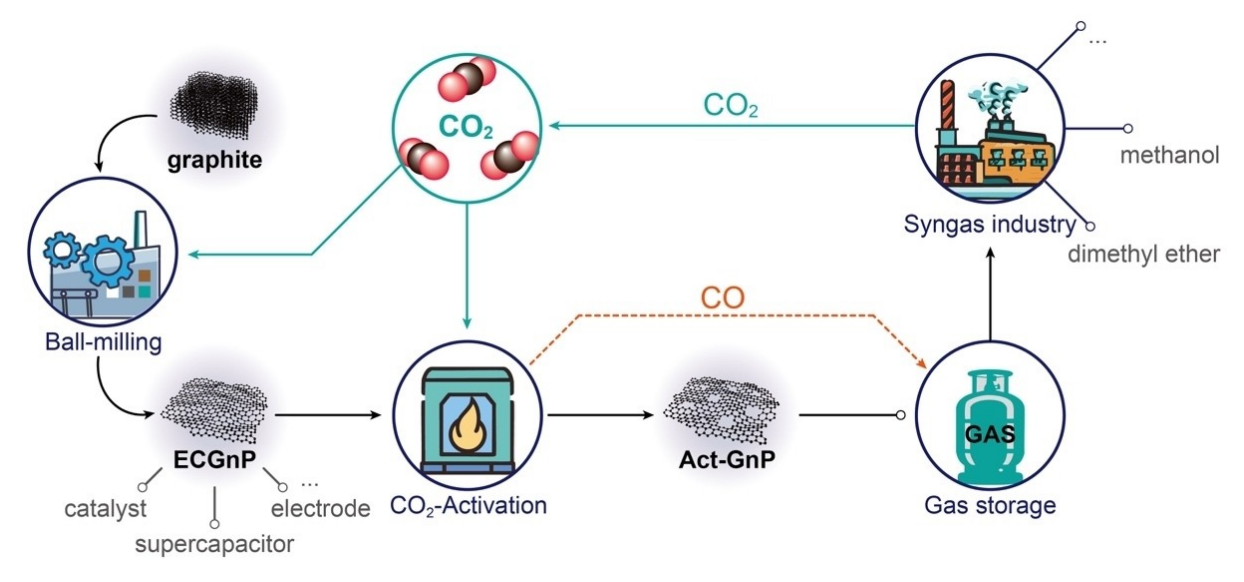


Figure 6. The sustainable production process of ECGnP to Act-GnP through mechanochemical preparation and the CO₂ utilization cycle.

4. Conclusions

In this study, we report the activation of ball-milled carbon (BMC) materials with CO₂ and investigate their gas storage performance. The CO₂-activated GnPs (Act-GnPs) exhibit a significant increase in surface area and tunable pore size compared to the pristine GnPs (or ECGnP). The Act-GnPs show an excellent gas storage performance for H₂, CH₄, and CO₂. The results suggest that CO2 activation offers a more environmentally friendly and cost-effective approach to producing high-performance ECGnPs for gas storage applications. Additionally, we anticipate that carbon structure modification could enhance catalytic activity in single-atom catalysts (SACs), representing a promising avenue for future research and application.[24-26] Furthermore, considering mass production, the exhausted CO/CO₂ mixture during the activation process promises to create a high-value-added chemical cycle with green hydrogen through the CO₂/syngas hydrogenation^[27-28] and electrochemical reactions. [29-30] Our findings demonstrate the potential of CO₂-activated GnPs for improving gas storage performance and advancing the development of carbon-based materials for energy-related applications.

Acknowledgements

This research was supported by Regional Innovation Strategy (RIS) through the National Research Foundation of Korea (NRF) funded by the Ministry of Education(MOE) (2023RIS-008).

Conflict of Interests

The authors declare no conflict of interest.

Data Availability Statement

The data that support the findings of this study are available from the corresponding author upon reasonable request.

Keywords: Gas adsorption ⋅ Porous carbon ⋅ Graphitic nanoplatelets, Activation · CO₂ utilization

- [1] I. Y. Jeon, Y. R. Shin, G. J. Sohn, H. J. Choi, S. Y. Bae, J. Mahmood, S. M. Jung, J. M. Seo, M. J. Kim, D. W. Chang, L. M. Dai, J. B. Baek, *Proc. Natl.* Acad. Sci. USA 2012, 109, 5588-5593.
- [2] S. J. Kim, G. F. Han, S. M. Jung, J. P. Jeon, S. H. Shin, S. W. Kim, I. Y. Jeon, J. B. Baek, ACS Nano 2019, 13, 5893-5899.
- [3] F. Li, G. F. Han, H. J. Noh, I. Ahmad, I. Y. Jeon, J. B. Baek, Adv. Mater. **2018**. 30. 1870330.
- [4] N. C. D. Nath, I. Y. Jeon, M. J. Ju, S. A. Ansari, J. B. Baek, J. J. Lee, Carbon 2019, 142, 89-98.
- [5] Z. C. Zhang, J. J. Sun, C. Lai, Q. Wang, C. G. Hu, Carbon 2017, 120, 411-418.
- [6] I. Y. Jeon, S. H. Shin, H. J. Choi, S. Y. Yu, S. M. Jung, J. B. Baek, Carbon 2017, 116, 77-83.
- [7] J. T. Xu, I. Y. Jeon, J. M. Seo, S. X. Dou, L. M. Dai, J. B. Baek, Adv. Mater. **2014**, *26*, 7317–7323.
- [8] I. Y. Jeon, M. Choi, H. J. Choi, S. M. Jung, M. J. Kim, J. M. Seo, S. Y. Bae, S. Yoo, G. Kim, H. Y. Jeong, N. Park, J. B. Baek, Nat. Commun. 2015, 6, 7123.
- [9] J. Xu, I. Y. Jeon, H. J. Choi, S. J. Kim, S. H. Shin, N. Park, L. M. Dai, J. B. Baek, 2D Mater. 2017, 4, 014002.
- [10] Z. Heidarinejad, M. H. Dehghani, M. Heidari, G. Javedan, I. Ali, M. Sillanpaa, Environ. Chem. Lett. 2020, 18, 393-415.
- [11] N. Byamba-Ochir, W. G. Shim, M. S. Balathanigaimani, H. Moon, Appl. Surf. Sci. 2016, 379, 331-337.
- [12] R. K. Liew, E. Azwar, P. N. Y. Yek, X. Y. Lim, C. K. Cheng, J. H. Ng, A. Jusoh, W. H. Lam, M. D. Ibrahim, N. L. Ma, S. S. Lam, Bioresour. Technol. 2018, 266, 1-10.
- [13] S. W. Choi, J. L. Tang, V. G. Pol, K. B. Lee, *J. CO*₂ *Util.* **2019**, *29*, 146–155.
- [14] L. L. Rao, S. F. Liu, L. L. Wang, C. D. Ma, J. Y. Wu, L. Y. An, X. Hu, Chem. Eng. J. 2019, 359, 428-435.
- [15] C. Bouchelta, M. S. Medjram, O. Bertrand, J. P. Bellat, J. Anal. Appl. Pyrolysis 2008, 82, 70-77.
- [16] R. Acosta, V. Fierro, A. M. de Yuso, D. Nabarlatz, A. Celzard, Chemosphere **2016**, *149*, 168–176.
- [17] M. Torkar, Eng. Failure Anal. 2006, 13, 624-628.
- [18] E. Rondero-Daniel, L. F. Diaz-Ballote, L. Maldonado-Lopez, A. Contreras, Rev. Mex. Fis. 2009, 55, 72-75.



- [19] M. Tangstad, J. P. Beukes, J. Steenkamp, E. Ringdalen in New Trends in Coal Conversion, (Eds: I. Suárez-Ruiz, M. A. Diez, F. Rubiera), Woodhead Publishing, 2019, pp. 405-438.
- [20] I.-Y. Jeon, H.-J. Choi, S.-M. Jung, J.-M. Seo, M.-J. Kim, L. Dai, J.-B. Baek, J. Am. Chem. Soc. 2013, 135, 1386-1393.
- [21] I.-Y. Jeon, H.-J. Choi, M. J. Ju, I. T. Choi, K. Lim, J. Ko, H. K. Kim, J. C. Kim, J.-J. Lee, D. Shin, S.-M. Jung, J.-M. Seo, M.-J. Kim, N. Park, L. Dai, J.-B. Baek, Sci. Rep. 2013, 3, 2260.
- [22] R. J. Dombrowski, D. R. Hyduke, C. M. Lastoskie, Langmuir 2000, 16, 5041-5050.
- [23] J. Mahmood, S. J. Kim, H. J. Noh, S. M. Jung, I. Ahmad, F. Li, J. M. Seo, J. B. Baek, Angew. Chem. Int. Ed. 2018, 57, 3415-3420.
- [24] S. Zhao, Y. Yang, Z. Tang, Angew. Chem. Int. Ed. 2022, 61, e202110186.
 [25] Y. Liu, C. Li, C. Tan, Z. Pei, T. Yang, S. Zhang, Q. Huang, Y. Wang, Z. Zhou, X. Liao, J. Dong, H. Tan, W. Yan, H. Yin, Z. -Q Liu, J. Huang, S. Zhao, Nat. Commun. 2023, 14, 2457.

- [26] J. Dong, Y. Liu, J. Pei, H. Li, S. Ji, L. Shi, Y. Zhang, C. Li, C. Tang, J. Liao, S. Xu, H. Zhang, Q. Li, S. Zhao, Nat. Commun. 2023, 14, 6849.
- [27] C. Du, P. Lu, N. Tsubaki, ACS Omega 2020, 5, 49-56.
- [28] X. Jiang, X. W. Nie, X. W. Guo, C. S. Song, J. G. G. Chen, Chem. Rev. 2020, 120, 7984-8034.
- [29] P. F. Wei, D. F. Gao, T. F. Liu, H. F. Li, J. Q. Sang, C. Wang, R. Cai, G. X. Wang, X. H. Bao, Nat. Nanotechnol. 2023, 18, 299-306.
- [30] X. L. Wang, J. F. de Araujo, W. Ju, A. Bagger, H. Schmies, S. Kuhl, J. Rossmeisl, P. Strasser, Nat. Nanotechnol. 2019, 14, 1063–1070.

Manuscript received: August 3, 2023 Revised manuscript received: February 28, 2024 Version of record online: April 5, 2024